CHAPTER 13

Shallow Landslide Delineation for Steep Forest Watersheds Based on Topographic Attributes and Probability Analysis

Jinfan Duan and Gordon E. Grant

13.1 INTRODUCTION

Mass movements triggered by rain and rain-on-snow events have been a major concern in forest management in many parts of the world (Sidle et al. 1985). Mass movements are dominant sources of sediment and affect the geometry and disturbance regimes of channel and riparian areas in steep forested lands (Swanson et al. 1987). Landslide-caused damage exceeds $1 billion annually in the United States (Schuster and Krizek 1978) and poses threats to life. Downstream effects of mass movements also affect water quality, water quantity, and aquatic habitat.

Landslides result from a combination of interacting factors that include topography; soil thickness, conductivity, and strength properties; rainfall intensity and duration; subsurface flow orientation; bedrock fracture flow; and vegetation surcharge and root strength (Montgomery and Dietrich 1994). These controlling factors are unevenly distributed in space and time, making quantitative assessment of landslide risk complex and difficult.

Mapping or delineating areas susceptible to landslides is essential for land-use activities and management decision-making in hilly and mountainous areas. Ideally, land-use activities, such as forest harvesting and road construction, should avoid vulnerable slope areas. Sites prone to mass failures can be identified by analytical and

Terrain Analysis: Principles and Applications, Edited by John P. Wilson and John C. Gallant.
ISBN 0-471-32188-5

empirical methods. A variety of approaches have been used in landslide mapping and can be classified into five categories: on-ground monitoring, remote sensing, factor overlay, statistical models, and geotechnical process models (Schuster and Krizek 1978). Each of these methods has its value for certain applications and disadvantages for other objectives (Ward et al. 1982, Montgomery and Dietrich 1994).

A computer-based framework incorporating topographic, vegetation, and soil information with geotechnical models is a useful way to locate unstable areas (Ward 1976, Okimura and Ichikawa 1985, Wu and Sidle 1995, Montgomery and Dietrich 1994). The recent trend of using spatially explicit approaches is largely due to the recognition of the importance of accounting for spatial heterogeneity, and newly developed tools and technology, especially geographic information system (GIS) and related remotely sensed imagery, and digital terrain analysis, which make it possible to consider small-scale heterogeneity. Incorporating digital terrain models into landslide prediction explicitly accounts for the importance of both topographic form and landscape position in slope stability. Recent work has demonstrated that both form and position represent first-order controls on landslide initiation (Dietrich et al. 1986, 1993, 1995, Montgomery and Foufoula-Georgiou 1993, Montgomery and Dietrich 1994, Zhang and Montgomery 1994).

Other studies have used spatial terrain data in regional stability analyses in conjunction with process-oriented models. Ward and co-workers (Ward 1976, 1985, Ward et al. 1978) delineate possible shallow landslide areas based on the uncertainties of control variables, but ignored the strong topographic control of shallow landslides by flow accumulation and convergence. Wu and Sidle (1995) developed an event-based slope stability model for forest watersheds, but the model is computationally intensive. Montgomery and Dietrich (1994) coupled near-surface flow characteristics with a slope stability model, but assumed steady-state rainfall and uniform soil and vegetation properties. Later work using the same model (Dietrich et al. 1995) explicitly accounted for both spatial variation in soil depth and the influence of root strength on slope stability. Their work did not, however, address the influence of temporally varying precipitation duration and intensities on slope stability.

In this chapter, we expand on these previous efforts to present a quantitative approach for evaluating both spatial and temporal factors influencing shallow landslides, using a more probabilistic framework than has previously been used. Topographic attributes from a digital elevation model (DEM) are linked with a process-based geotechnical equilibrium model. In this model, the high variability of factors controlling landslide occurrence and temporal variability of subsurface saturation are treated using probability analyses. Our intent is to explore an alternative representation of the uncertainty and variability inherent in simulating climatic and topographic controls on landslide initiation. This representation includes a dynamic simulation of rainfall intensities and treats the spatial distribution of key soil parameters stochastically, using a Monte Carlo simulation approach.

The following sections describe the study area, the theory underlying the model, model parameterization, and results of testing it using data on observed landslides in

a 64-km^2 watershed in western Oregon. We conclude with a discussion that considers the advantages and disadvantages of this approach with respect to other models that predict landslide location and frequency.

13.2 STUDY AREA DESCRIPTION

We tested the model against landslide inventory data from the H. J. Andrews Experimental Forest (hereafter HJA) in the western Cascade Range of Oregon. The HJA includes the 64-km^2 drainage basin of Lookout Creek, a tributary of the Blue and McKenzie rivers (Figure 13.1). Elevations range from 410 to 1630 m.

Lower elevations of the HJA are underlain mainly by Oligocene and lower Miocene volcanic rocks composed of tuffs, ash flows, and stream deposits. In higher areas, bedrock is composed of andesite lava flows of Miocene age and of younger High Cascade rocks. Stream erosion, a variety of types of landsliding, and glaciations have created a deeply dissected, steep landscape. Soils developed in these parent materials are mainly Inceptisols with local areas of Alfisols and Spodosols. Field estimation of soil depth over the Andrews Forest from soil pits found a pattern of thick soils in the upper two-thirds of the basin, which is underlain by deep-seated earth flows, with thinner soils in the lower elevation zone. Thick alluvium borders many of the lower-elevation streams (Dyrness 1969) (Figure 13.2). Soil depth is quite

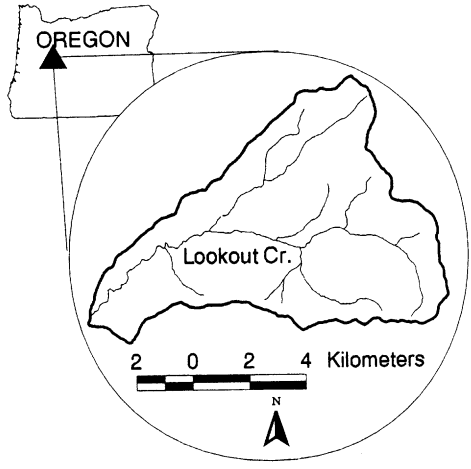

Figure 13.1. Location of the H. J. Andrews Experimental Forest, comprising the Lookout Creek watershed. Shaded areas show gauged watersheds with long-term stream flow and climate observations.

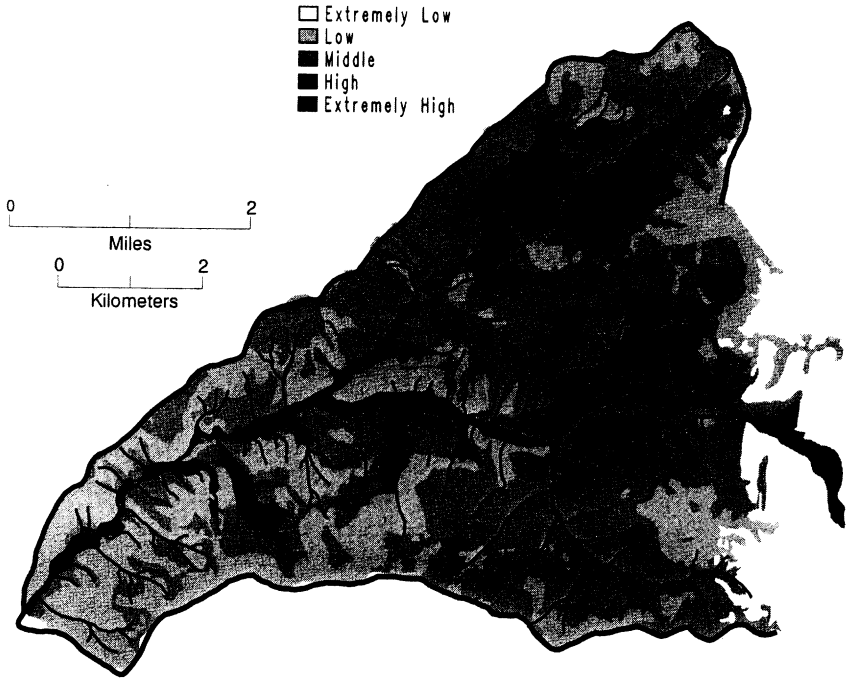

Figure 13.2. Soil depth in the H. J. Andrews Experimental Forest.

variable locally and, because of the extensive mass movement history of the area, does not always conform to topography.

The maritime climate has wet, mild winters and dry, cool summers. At the primary meteorological station at 430 m elevation, mean monthly temperature ranges from near 1°C in January to 18°C in July. Average annual precipitation varies with elevation from about 2300 mm at lower elevations to over 3500 mm at upper elevations, falling mainly from November through March. Rain predominates at low elevations; snow is more common at higher elevations. Highest stream flow occurs generally from November through February during warm rain-on-snow events.

When it was established in 1948, the Andrews Forest was covered with old-growth forest. Douglas fir, western hemlock, and western red cedar dominate lower elevation forests. Upper elevation forests contain noble fir, Pacific silver fir, Douglas fir, and western hemlock (Figure 13.3). Before timber cutting began in 1950, about 65% of the Andrews Forest was in old-growth forest (400–500 years old) and the remainder was largely in stands developed after wildfires in the mid 1800s to early

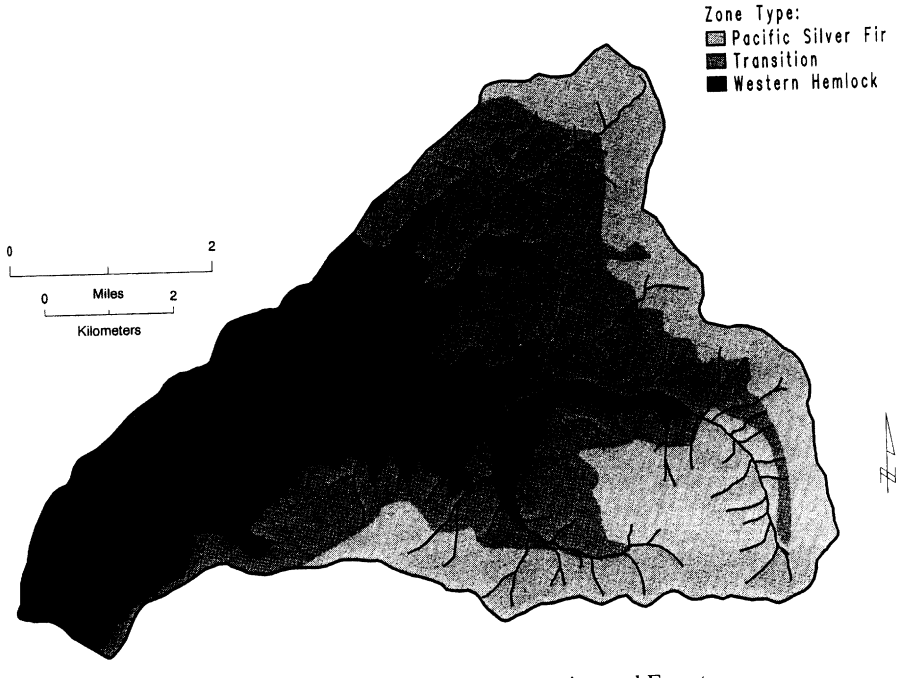

Figure 13.3. Vegetation zones in the H. J. Andrews Experimental Forest.

1900s. Clear-cutting and shelterwood cuttings over about 30% of the Andrews Forest have created young plantation forests varying in composition, stocking level, and age (Figure 13.4). Old-growth forest stands with dominant trees over 400 years old still cover about 40% of the total area. Mature stands (100 to 140 years old) originating from wildfire cover about 20%. Wildfire was the primary disturbance in the natural forest; windthrow, landslides, sites of concentrated root rot infection, and lateral stream channel erosion were secondary disturbances.

13.3 METHODS AND DATA SOURCES

To delineate landslide-prone areas, the infinite slope model was coupled with a probabilistic analysis of precipitation and landscape parameters. This approach is discussed in the following sections.

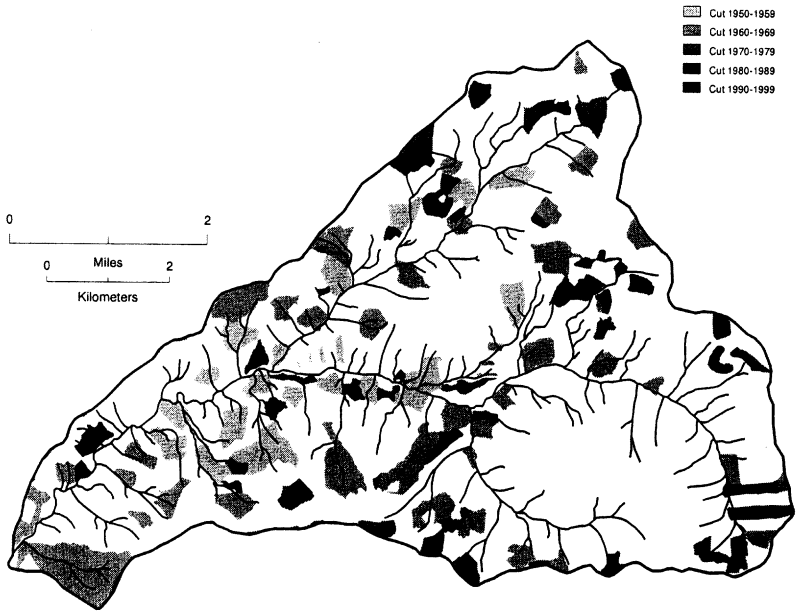

Figure 13.4. Land-use history in the H. J. Andrews Experimental Forest.

13.3.1 Infinite Slope Model

The factor of safety (FS) is commonly used as a quantitative expression of the hazard index of landslide initialization. It is customarily expressed as the balance between resisting and driving forces such that

$$FS = \frac{\text{Resistance of the soil to failure (shear strength)}}{\text{Forces promoting failure (shear stress)}} \tag{13.1}$$

In equilibrium analysis, an FS of unity is a critical condition and would indicate imminent failure, and an FS greater than one indicates a stable condition. The infinite slope method is a popular slope stability analysis tool because it is simple and applicable to many shallow landslides. Generally, the infinite slope model does not adequately predict deep-seated, rotational failures, but is appropriate for failures of a soil

mantle that overlies a sloping drainage barrier that may be bedrock, or a less permeable and well-compacted soil layer (Hammond et al. 1992).

A variety of slope stability models characterize stability using factor of safety. The infinite slope model is widely used (e.g., Ward 1985, Wu and Sidle 1995, Montgomery and Dietrich 1994). It can be written as

$$FS = \frac{C + \Delta C_r + \{[(D-h)\gamma_m + h(\gamma_{sat} - \gamma_w)] + W_r\} \cos\beta \tan\phi}{[(D-h)\gamma_m + h\gamma_{sat} + W_r] \sin\beta} \quad (13.2)$$

where C is soil cohesion; ΔC_r is root strength; W_r is the surcharge weight of vegetation; γ_m and γ_{sat} are the unit weight of soil at field moisture content and saturation, respectively; D is the soil depth normal to the slope; h is the normal saturated depth; β is the surface slope; and ϕ is the internal frictional angle.

13.3.2 Parameter Estimation from Probability Analysis

Hillslopes commonly have a variety of rock types, soils with different properties and thicknesses, and vegetation with different surcharges and root strengths. Deterministically quantifying all these controlling factors is impossible for regional hazard mapping. Quantifying error and determining error sources and uncertainties are difficult, if not impossible. Many model equations may be inappropriate, because they may only be used for defined boundary conditions at specific scales: Equation 13.2, for example, is not valid for deep-seated earthflows. Even if measurement errors are assumed negligible and back-calculation of parameters is well defined, point measurements (e.g., strength tests) cannot effectively describe the larger-scale heterogeneity of the measurable parameters, such as frictional angle and cohesion.

Because the parameters in Equation 13.2 are inherently uncertain, a probability of failure for each hillslope element must be estimated (Ward et al. 1982) rather than predicted deterministically. In fact, the predictions of landslide occurrence from simple deterministic models actually represent statements of probability (Montgomery and Dietrich 1994). Some parameters that are highly variable in space and time, including soil and root strength, soil depth, and saturated depth, can be considered as random variables or assumed to be uniform (as we do for all but saturated depth). Other parameters, such as slope angle and unit weight of soil, can be estimated with greater accuracy from terrain analysis and/or GIS software, or from field surveys. In some landscapes, factors such as soil depth are strongly correlated with topography (i.e., Dietrich et al. 1986, 1995); however, this assumption is less valid in our landscape because of extensive mass movement and glacial overprinting.

Two important assumptions simplify the problem. First we treat the highly variable parameters as independent, following Ward et al. (1982), while recognizing that some of the stochastic variables in the infinite slope model are correlated (Hammond et al. 1992). There is no good way to handle this dependency quantitatively: Typically, soil cohesion and friction angle are inversely related (correlation coefficient of

−0.2 to −0.85) (Cherubini et al. 1983), while friction angle and soil density are positively related (Hammond et al. 1992). Although Hammond et al. (1992) adopted methods using transformed variables to treat the correlations between soil cohesion and friction and between friction angle and soil density, further research is needed to evaluate the statistical soundness and general applicability of this approach.

The second assumption involves using prior assigned distributions for certain parameters. In this chapter, all variables except saturated depth are based on an assumed uniform distribution (Ward et al. 1978) (Table 13.1). Saturated depth is affected by various factors, such as precipitation, evapotranspiration, vertical recharge, and deep ground water seepage, that are controlled by soil and vegetation characteristics. Based on the concept of the time–area curve and hillslope unit hydrograph (Iida 1984), Barling et al. (1994) derived a quasi-dynamic relationship between recharge rate and the saturated depth as

$$h(t) = \frac{r}{K_s \tan \beta} a(t) \tag{13.3}$$

where $h(t)$ denotes the depth of saturated throughflow at time t; r is the constant recharge rate; $a(t)$ is the upslope drainage area divided by the downward width of the element in this case; and K_s is the saturated conductivity of soil.

The assumption of uniform recharge rate is only a simplification of the complex behavior of the soil–vegetation–atmosphere interface. If we further ignore canopy interception and evapotranspiration loss, r can be viewed as the precipitation mean intensity, I_m, which we define as an exponential distribution (e.g., Beven 1987):

$$f(I_m) = \frac{e^{-I_m/\lambda_P}}{\lambda_P} \tag{13.4}$$

where $f(I_m)$ denotes a probability density function and λ_P is mean storm intensity, in mm/h.

TABLE 13.1 Stochastically Treated Parameters and Their Assumed Probability Distributions

Random Variable	Probability Distribution
Soil depth	Uniform
Soil cohesion	Uniform
Internal friction angle	Uniform
Root strength	Uniform, mean dynamic change with age
Biomass surcharge	Uniform, mean dynamic change with age
Precipitation intensity	Exponential

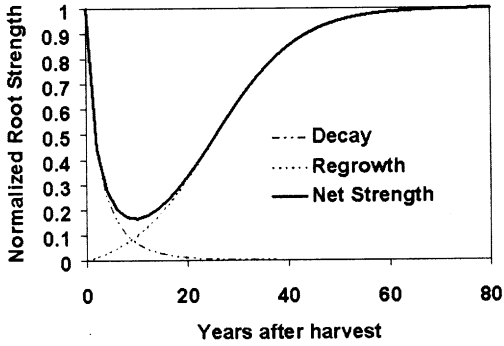

Figure 13.5. Root strength change after forest cutting. Only the mean is shown; variance is assumed constant for different years after cutting.

13.3.3 Effect of Vegetation

Vegetation influence on slope stability is also an important factor in steep forested watersheds, especially through root strength (Sidle 1992). Tree roots provide lateral support and vertically anchor and buttress the soil mass (Hammond et al. 1992). A sigmoid curve was used to model root cohesion during regrowth (Sidle 1992); an exponential curve was used to model the decay of residual root strength following tree harvesting (Sidle 1992) (Figure 13.5). The general shape of conceptual root strength regeneration is

$$C_r = C_{max}\,[(a_r + b_r e^{-k_r t})^{-1} + d_r] \tag{13.5}$$

and the root deterioration is

$$C_{rd} = C_{max}\, e^{-K_d t^{m_1}} \tag{13.6}$$

Total root strength is given as

$$\Delta C = C_r + C_{rd} \tag{13.7}$$

where a, b, d, m, and k are all parameters (Sidle 1991, 1992) and C_{max} is the maximum root strength.

Biomass surcharge is generally not a significant factor in landslide initiation (Hammond et al. 1992). We include it, however, because it is explicitly influenced by both timber harvest and tree regrowth and may affect the stability threshold at which sliding occurs on marginally stable sites. Different functions have been used for calculating biomass after harvesting. A function similar to the root regrowth Equation (13.5), as described by Sidle (1987), is used here (Figure 13.6):

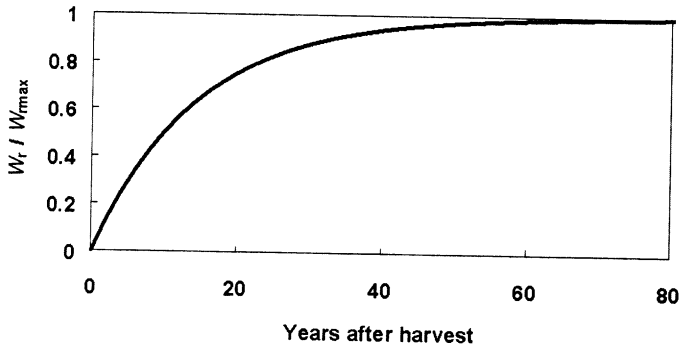

Figure 13.6. Biomass surcharge after forest cutting. Only the mean is shown; variance is assumed constant for different years after cutting.

$$W_r = W_{max}\left[(a_w + b_w e^{-k_w t})^{-1} + d_w\right] \tag{13.8}$$

where W_r is the biomass over the element at t years after cutting; W_{max} is the maximum weight trees can grow in unit area; and a_w, b_w, c_w, and d_w are constants. As indicated by Sidle (1992), the model assumes that tree surcharge is uniformly distributed across each element.

Based on the above equations characterizing the changing vegetation factors after harvesting, we obtain the means of the uniform distribution for onsite root cohesion and biomass surcharge. The variances of these two distributions are treated as constants equal to one-tenth of the normalized root cohesion and biomass.

13.3.4 Terrain Analysis and Climate Data Acquisition

The data and parameters used for this investigation were derived from or obtained by existing Level 1 DEM, aerial photograph and field surveys. The DEM data stored in the ARC/INFO GIS have a resolution of 30 × 30 m and the slope and topographic convergence index were computed for each pixel using internal GIS functions. Although considering flow as multidirectional out of each pixel is more sophisticated conceptually, the GIS tool we used incorporated only a single-direction algorithm. Because this algorithm accumulates drainage area only along cardinal directions and 45° to those directions, it inevitably results in the "striping" artifacts visible on Figures 13.8 and 13.9. Newer flow-routing algorithms, like those discussed in Chapters 3 and 5, may eliminate this problem.

The soil and vegetation characteristics and the land-use history were rasterized to the DEM resolution in ARC/INFO. For the seven soil types that occupy most of the area of HJA, parameters of soil strength and saturated conductivities were derived from field measurements (Table 13.2), and the average of the known seven types was used for the remaining unmeasured types. The error introduced by this method is limited because of the small area involved. Although there are three vegetation zones at HJA, we used the same vegetation parameters for all types in the random simulation

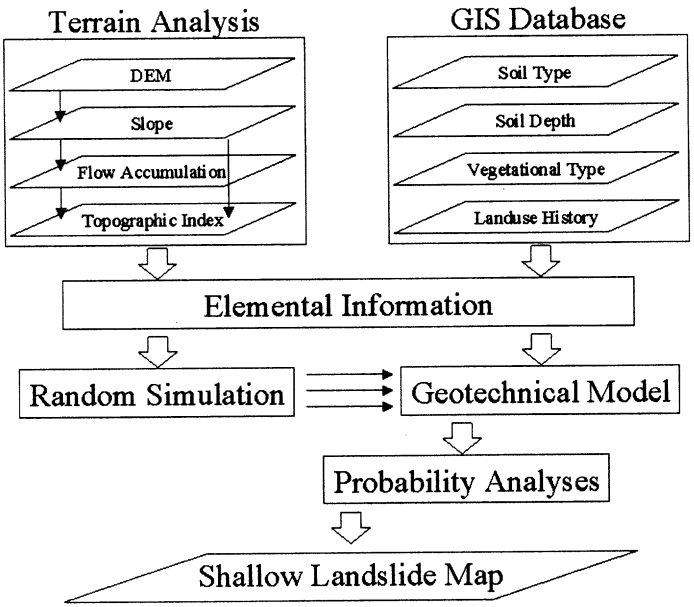

Figure 13.7. General simulation procedure.

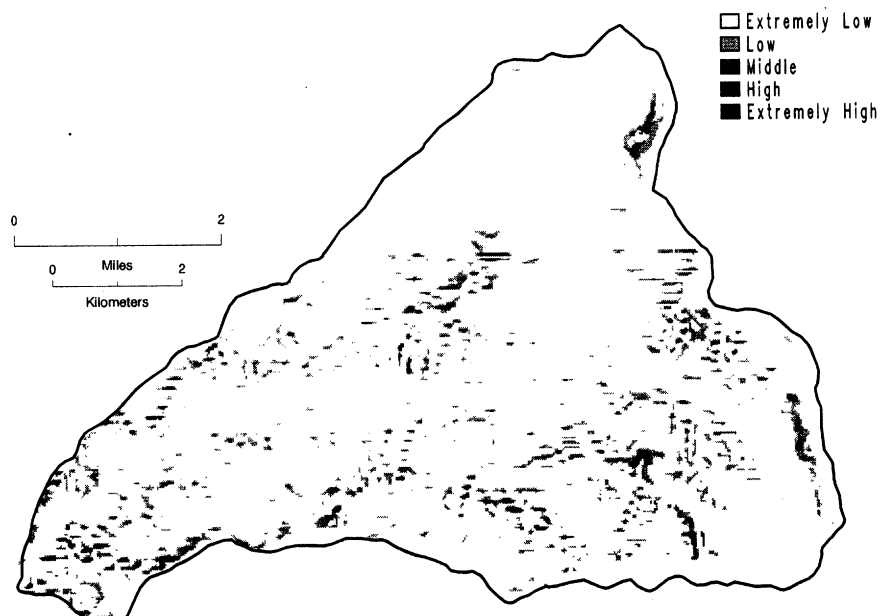

Figure 13.8. Potential shallow landslide area in the H. J. Andrews Experimental Forest under old-growth condition.

TABLE 13.2 Soil Parameters Used in Model Test

Soil Parameters	*Soil Type*								*Reference*
	Flunky	Blue River	Limberlost	Budworm	Slipout	Frissell	Mckenzie	Others	
Bulk density (g/cm^3)	2.317	1.034	1.421	1.564	1.477	1.954	1.585	1.6002	Rothacher et al. 1967
Porosity (vol/vol)	0.29	0.63	0.52	0.5	0.48	0.4	0.53	0.486	Rothacher et al. 1967
Field capacity (vol/vol)	0.102	0.285	0.277	0.324	0.343	0.217	0.265	0.2852	Rothacher et al. 1967
Saturated conductivity (m/s)	0.004178	0.001567	0.002089	0.001567	0.000627	0.000627	0.000418	0.001044	Calibrated
Cohesion (kPa)					0–15				Hammond et al. 1992
Frictional angle (°)					30–45				Hammond et al. 1992

TABLE 13.3 Vegetation Parameters Used in Model Test

Parameters	Value Used	Reference
Root strength		Sidle 1991
C_{max}, maximum (kPa)	12.5	
k_d, coefficient in residual	0.402	
m_1, coefficient in residual	0.647	
a_t, coefficient in regrowth	0.952	
b_t, coefficient in regrowth	19.05	
d_r, coefficient in regrowth	–0.05	
k_r, coefficient in regrowth	0.12	
Biomass		Oral communication with Harmon 1995, Sidle 1992
W_{max}, maximum (kPa)	3	
a_w, coefficient	0.952	
b_w, coefficient	19.05	
c_w, coefficient	–0.05	
k_w, coefficient	0.12	

because the root strength and biomass surcharge values were similar among types (Table 13.3).

Storms were defined as periods with a mean precipitation intensity greater than 1 mm h^{-1}, separated by at least 12 h with precipitation less than 1 mm h^{-1} (Beven 1987). We analyzed precipitation records for the climate station that has the longest history of observation at HJA over a 36-year period (water year 1958 to 1993). A total of 1097 storms fitting the above criteria had an average intensity of 1.35 mm h^{-1}.

13.3.5 Monte Carlo Simulation and Probability Derivation

The simulation of probability of landslide occurrence relies on spatially distributed information of small elements. From terrain analysis and GIS, topographic attributes such as slope, flow accumulation and topographic convergence index can be derived from the DEM for each element. Overlaying the distributed elements with a GIS database helps with the derivation of other land surface or near-surface characteristics, such as soil, vegetation and land-use history (Figure 13.7).

For each element, 1000 random simulations were produced that represented the ranges in probable value of saturation, soil and root strength, and biomass, using the appropriate probability distributions (Tables 13.1 and 13.2). The variables in Table 13.1 were treated as random variables, which means we randomly simulated them, using the assumed probability distribution and the mean and variance calculated from the terrain and precipitation data. For each simulation set of these variables, a factor of safety was calculated based on the geotechnical model (Equations

13.2–13.4). Then the mean (μ_{FS}) and variance (σ_{FS}) of factor of safety from the Monte Carlo simulation for each element were computed. By assuming a normal distribution for the factor of safety (Ward et al. 1982), the probability of failure, defined as the probabilities of factor of safety less than and equal to 1 for each element, was calculated using the normal probability distribution:

$$P(\mathrm{FS} \le 1.0) = \int_{-\infty}^{1.0} \frac{1}{\sqrt{2\pi}\sigma_{FS}} \exp\left[-\frac{1}{2}\left(\frac{x-\mu_{FS}}{\sigma_{FS}}\right)^2\right] dx \qquad (13.9)$$

which can be solved numerically. Another way to construct the probability of failure is to use the ratio of the number of sets with computed FS less than or equal to one divided by total number of Monte Carlo simulation sets. The latter has the advantage of not assuming a distribution for factor of safety. Our tests demonstrated that when large numbers of simulation sets are computed, there is little difference in the resulting slide maps between these two methods.

The 1000 simulations for each element were constructed based on the random parameters of soil, vegetation, and precipitation characteristics, using Equations 13.3 and 13.4. The probability of failure was computed for each element using the simulation. Two conditions were considered: First, we analyzed probability of failure for old-growth conditions; second, we examined the probability of failure at 12 years post clear-cutting for the whole watershed, when root strength is usually at a minimum and the landscape is, therefore, most unstable following cutting.

We qualitatively define the probability of slope movement as extremely low ($P \le 0.2$), low ($0.2 < P \le 0.4$), moderate ($0.4 < P \le 0.6$), high ($0.6 < P \le 0.8$), and extremely high ($0.8 < P \le 1.0$). This relative ranking of stability of hillslope elements does not have an absolute timescale attached to it. However, since the 36-year climate record used to generate the precipitation input incorporates events ranging up to approximately a 100-year return period, the implied timescale is of one to several centuries in length. This corresponds closely with the interpreted return period of sliding for topographic hollows with mature forest cover of several hundred years in this area (Swanson et al. 1987).

13.4 RESULTS AND DISCUSSION

The two modeled vegetation conditions yielded dramatically different patterns of landslide probabilities (Figures 13.8, 13.9). Under old-growth conditions most of the hillslopes are stable and only scattered areas have a high potential for shallow landslides (Figure 13.8). Under old-growth conditions, 98% of the area is stable; 92% of the areas is ranked extremely low in probability of failure (Figure 13.10). Only 1% of the uncut forest has a high probability of sliding and none is rated extremely unstable. Under clear-cut conditions, on the other hand, only 76% of the area is rated in a stable state; the area with high failure probability has increased to 11%, with 3% of the area ranked as extremely unstable under the recent clearcut condition. Under both

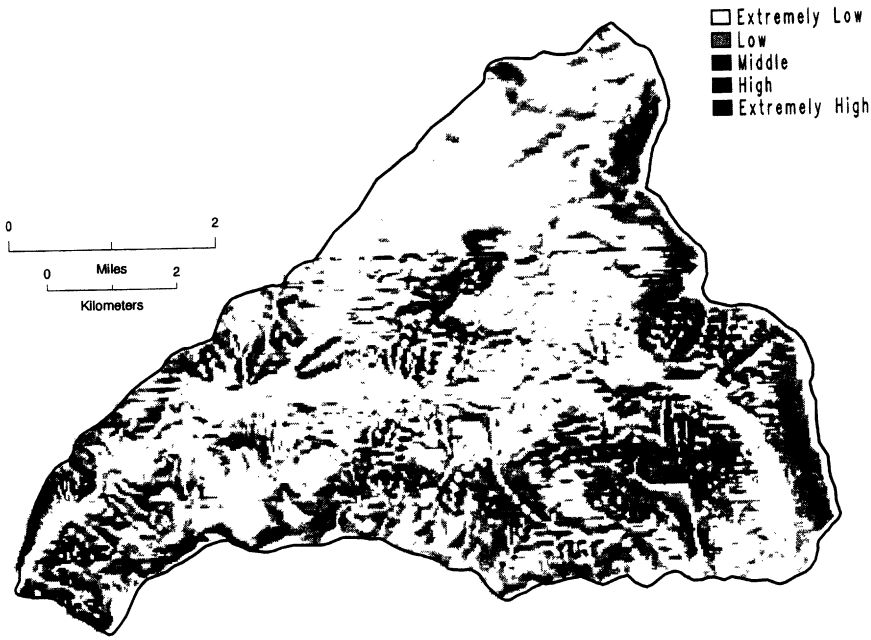

Figure 13.9. Potential shallow landslide area in the H. J. Andrews Experimental Forest under condition that the whole drainage is clear-cut.

scenarios, the proportion of area in each category declines exponentially with increasing landslide risk.

Historically, approximately 137 landslides occurred at the HJA (Figure 13.11) (F. Swanson, unpublished data on file at Pacific Northwest Research Station). Of these 137 slides, 71 (52%) are road-related and 35 (25%) are clear-cut-related, with another 31 (23%) in forest. This inventory clearly demonstrates the acceleration of

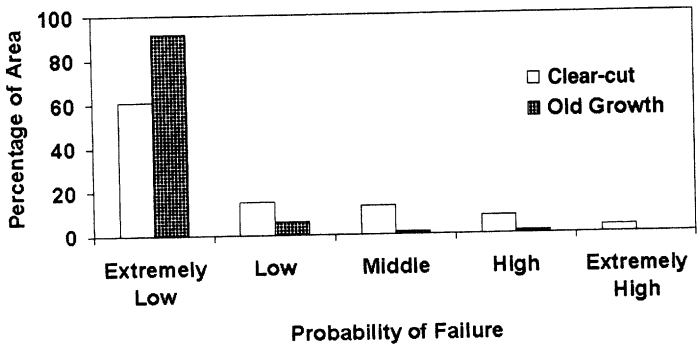

Figure 13.10. Percentage of areas under different slide potential categories for old growth and clear-cut.

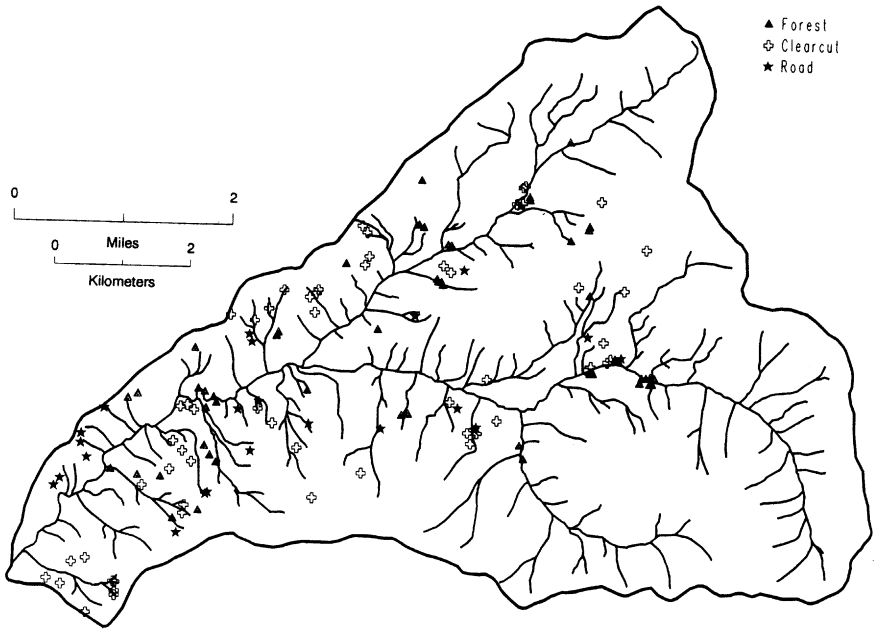

Figure 13.11. Observed landslide sites and associated land use conditions for 1950–1990.

landsliding due to road construction and cutting at HJA (Swanson and Dyrness 1975). Comparison of observed landslide sites with predicted unstable areas for current land-use conditions, incorporating existing vegetation cutting patterns (but not roads) (Figure 13.12), can be used to test model performance. Table 13.4 compares the modeled and observed landslide sites based on a point registration that treats any landslide site as a single point in the spatial database.

Overall, the model does not predict the observed sliding behavior very well. Many landslides occurred at elements mapped as low-probability areas. These discrepancies may be due to several factors, which point to the limitations of this model or landslide models in general for accurately predicting slide locations. A key limitation may be errors related to accurately pinpointing landslide sites as points in GIS coverages. Average areas for individual slides are approximately 200–300 m^2, assuming an average slide depth of 2 to 3 m (Swanson and Dyrness 1975); so that the slide area is less than the 900 m^2 (30 × 30 m) "window" generated with 30 m square-grid DEMs. Given the uncertainties attached to both accurately locating field-inventoried slides on the DEM as well as pinpointing them with the model, a more robust test might utilize a larger (e.g., 3 × 3 cell) window, associating slide risk with the highest probability recorded in any of the 9 cells. A related critical factor is the coarseness of the DEM data itself; 30-m data do not typically display the topographic detail that drives landsliding (Zhang and Montgomery 1994). The single-flow-direction algorithm used to calculate drainage area also imposes an artificial structure that may influence predictions in unknown ways.

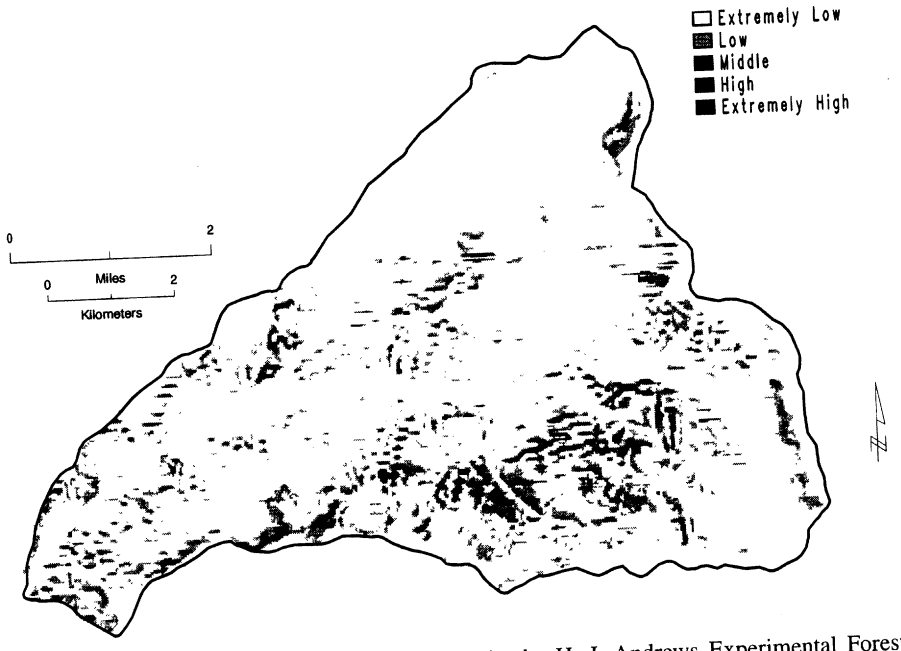

Figure 13.12. Potential shallow landslide area in the H. J. Andrews Experimental Forest under current stand conditions.

More importantly, this model does not incorporate geologic information, which plays an important role in the geographic pattern of shallow landslides. The model overestimates the landslide potential for high-elevation areas of the HJA, where competent andesite lava flows underlie the hillslopes. Soil developed from this rock type typically has a very high rock content and therefore does not build the high pore pressures necessary to trigger landslides. Another consideration is that many landslides occur during rain-on-snow events, which typically occur in lower to middle elevation areas. The model does not consider that high-elevation areas may have snowpacks that persist through storms (Swanson and Dyrness 1975). Nor does it explicitly consider the contribution of roads and associated altered drainage patterns to slope stability. Finally, 50% of the landslides observed within the 40-year inventory period occurred during two storms in the winter of 1964–65. The climatologic conditions necessary to trigger major episodes of landsliding are probably underrepresented by the probabilistic simulation of precipitation.

TABLE 13.4 Percentage of Observed Slide Sites and Delineated Probability for Different Land-Use Categories

	Extremely Low	Low	Middle	High	Extremely High
Road	60	21.5	13.8	3.1	1.5
Clear-cut	67.6	8.8	20.6	2.9	0
Forest	62.5	31.3	0	6.3	0

Other mass movements, such as earth flows, are present at HJA, in addition to shallow debris slides. The infinite slope model used in this project is valid only for shallow landslides and not for deep-seated earth flows. Other types of topographically controlled representations are needed to delineate deep slides.

Because of these factors, agreement between the model and inventory data is only fair. Future models for this area must explicitly consider the effects of geology on soil strength and hydraulic conductivity. A simple partitioning of the HJA basin by geology alone gave much better agreement with actual slide data (Swanson and Dyrness 1975). This raises the possibility that model performance might be improved if geologic variation were explicitly considered in the model, perhaps by defining ranges for soil cohesion based on geology. However, poor resolution of soil mapping due to dense forest cover contributes to uncertainties in defining soil and geological properties, however.

13.5 IMPLICATIONS FOR MANAGEMENT AND FUTURE MODELING

The relatively poor fit to the observed data, together with uncertainties as to how to interpret goodness-of-fit in the first place, raises interesting questions regarding how mixed dynamic and probabilistic models like this one, or other more deterministic models (i.e., Montgomery and Dietrich 1994), should be used in management applications. Use of topographically driven landslide models in land-use management is still rather new. Increasing concern about accelerated risks from landsliding following forest harvest, however, is prompting managers to look for more sophisticated tools to predict location and probability of failures. Understanding the strengths and limitations of these models is therefore crucial.

Both deterministic and probabilistic models must address the inherent uncertainty in predicting parameters controlling slide initiation; these parameters include both climatic and topographic variables. Measures of model success can include the spatial pattern of slides, the timing with respect to triggering storms, and the overall slide frequency integrated over multiple years or decades.

In general, the success rate for predicting slide *location,* as measured against observed slide locations, appears to be greater for the more deterministic models. Even simple models that incorporate the strong topographic controls on landslide location (i.e., convergent topography and hillslope gradient) appear to predict the overall spatial pattern of slides rather well, where sliding is primarily controlled by topography (Montgomery and Dietrich 1994, Dietrich et al. 1995). These models have been less well-tested in terrain such as the H. J. Andrews, where deep-seated earth flows introduce other factors controlling sliding (i.e., long-term mass movement history) that are not well-represented by topography. The Monte Carlo approach described here does less well, perhaps because the key variables influencing slide initiation that were simulated, such as soil and root strength, are not truly random but are topographically controlled as well. Land-use decisions requiring maps that broadly predict landslide risk and slide-prone sites would do well to rely on the more deterministic models, as long as underlying assumptions of mechanisms responsible for slide initiation were not violated.

Predicting slide frequencies, either at an event (i.e., individual storm) or longer-term (i.e., multiyear) timescale, however, may require better representation of climatic forcing functions, since landslide initiation may be due as much to transient precipitation intensities as to average or mean precipitation amounts. The theoretical distribution of precipitation events utilized here is a first attempt to explicitly incorporate a more detailed hydrology into landslide models. The increased value of this approach in terms of predictive power, however, is hard to demonstrate because all the other sources of uncertainty and error obscure any incremental gains. Future work should focus on testing model predictions of landslide frequencies at both event and decadal timescales.

13.6 CONCLUSIONS

The model described here explicitly considers the spatial heterogeneity of landscape characteristics, such as soil and root strength, using Monte Carlo simulation. Precipitation events, the most influential variable on landslide frequency and timing, are also stochastically treated based on a theoretical exponential distribution. The advantage of the probabilistic approach is that it may offer a less biased way of distributing inherent uncertainties across the landscape. Whether this necessarily results in an increase in ability to predict either timing or location of slides remains to be seen.

As expected, this topographically explicit method is strongly influenced by terrain-analysis methods (e.g., grid-based versus contour-based methods, single flow direction versus multiple flow direction algorithms). Different terrain-analysis methods produce distributed elements of different sizes and shapes that reflect different topographic attributes, such as slope, aspect, and drainage area, hence landslide probability. Future research should also explore the influences of different terrain-analyses methods, scale, and DEM data quality on landslide delineation.